EFDA–JET–PR(09)05

G.S. Xu, V. Naulin, W. Fundamenski, C. Hidalgo, J.A. Alonso, C. Silva,
B. Gonçalves, A.H. Nielsen, J. Juul Rasmussen, S.I. Krasheninnikov,
B.N. Wan, M. Stamp and JET EFDA contributors

Blob/Hole Formation and Zonal Flow Generation in the Edge Plasma of JET Tokamak

Blob/Hole Formation and Zonal Flow Generation in the Edge Plasma of JET Tokamak

G.S. Xu[1,2], V. Naulin[3], W. Fundamenski[1], C. Hidalgo[4], J.A. Alonso[4], C. Silva[5], B. Gonçalves[5], A.H. Nielsen[3], J. Juul Rasmussen[3], S.I. Krasheninnikov[6], B.N. Wan[2], M. Stamp[1] and JET EFDA contributors*

JET-EFDA, Culham Science Centre, OX14 3DB, Abingdon, UK

[1]EURATOM-UKAEA Fusion Association, Culham Science Centre, OX14 3DB, Abingdon, OXON, UK
[2] Institute of Plasma Physics, Chinese Academy of Sciences, Hefei 230031, China
[3] Association Euratom-Risø DTU, DK-4000 Roskilde, Denmark
[4] Laboratorio Nacional de Fusión, Euratom-Ciemat, 28040 Madrid, Spain
[5] Euratom-IST, Avenida Rovisco Pais, 1049-001 Lisbon, Portugal
[6] University of California, San Diego, California 92093, USA
** See annex of F. Romanelli et al, "Overview of JET Results",*
(Proc. 22 [nd] IAEA Fusion Energy Conference, Geneva, Switzerland (2008)).

Preprint of Paper to be submitted for publication in
Nuclear Fusion Letter

ABSTRACT.
First experimental evidence showing the connection between blob/hole formation and zonal flow generation was obtained in the edge plasma of the JET tokamak. Holes as well as blobs are observed to be born in the edge shear layer, where zonal flows shear off meso-scale coherent structures, leading to disconnection of positive and negative wave crests. The newly-formed blobs transport azimuthal momentum up the gradient of the azimuthal flow and drive the zonal-flow shear while moving outwards. During this process energy is transferred from the meso-scale coherent structures to the zonal flows via the turbulent Reynolds stress, resulting in nonlinear saturation of edge turbulence and suppression of meso-scale fluctuations. These findings carry significant implications on the mechanism of structure formation in magnetically confined plasma turbulence.

1. INTRODUCTION

Blobs are observed as magnetic-field-aligned filaments, or meso-scale coherent structures of excess density and temperature as compared to the background plasma, while holes are coherent structures of reduced density and temperature. They are propelled through the plasma by a charge polarization induced by magnetic curvature and gradient drifts and a corresponding **E**×**B** radial convection reacted to satisfy quasineutrality. The study of plasma blobs and the resultant intermittent convective transport is one of the most active research areas within plasma physics, not only because blobs are believed to dominate the transport across the Scrape-Off Layer (SOL) of fusion devices and possibly lead to serious wall erosion, impurity and recycling problems for future fusion reactors, but also because it seems to be a universal phenomenon found irrespective of the details of the magnetic geometries, devices, parameters, as well as the underlying instability driving forces or dissipation processes [1]. Similar propagating coherent objects have also been observed in the ionosphere [2] and in the solar photosphere [3]. The remarkable universality of such phenomena in plasma turbulence suggests they possibly have the same nonlinear origin. While substantial progress has been made in understanding the radial motion of blobs [4], the mechanism(s) of blob/hole formation still remains an open question [1]. Blob transport has been investigated experimentally in TCV [5] and JET tokamaks [6]. Recent experimental results from a simple magnetized torus shed some light on the mechanism of blob formation [7]. These preliminary observations are generally supported by the theories and simulations [8-11], although differing in detail.

In this letter, first experimental evidence from a fusion device showing the connection between blob/hole formation and zonal flow generation is presented. Holes as well as blobs are observed to be born in the Edge Shear Layer (ESL) where zonal flows [12] shear off meso-scale coherent structures, leading to disconnection of positive and negative wave crests. The interchange drive causes the newly-formed coherent objects to move: blobs move downhill (outwards) and holes move uphill (inwards), so that accumulated regions of blobs and holes are formed on each side of the shear layer. Only those big (with radial extent $\lambda_r \geq \delta_r$, where δ_r is ESL width) and stable (with structure lifetime $\tau_{life} \geq \tau_{shear} \equiv \lambda_\theta / (\lambda_r \delta_r V_\theta)$ [13], where τ_{shear} is shear decorrelation time, λ_θ is

structure poloidal size or wavelength, $\delta_r V_\theta$ is poloidal-flow shear rate) structures can finger out of the ESL, be sheared off and become blobs. Small structures die before escaping from the shear region because of their short lifetime. Eventually, a blob is peeled off from the bulk plasma, moves into the SOL and leaves a hole behind. The newly-formed blobs carry azimuthal momentum up the gradient of the azimuthal flow while moving outwards. During this process zonal flows are generated through the tilting mechanism [14] mainly associated with the meso-scale coherent structures. Energy is inverse-cascaded from these structures to the zonal flows via turbulent Reynolds stress ($\Pi_{\mathrm{Re}} \equiv \langle v_r v_\theta \rangle$) [12], resulting in nonlinear saturation of edge turbulence and suppression of meso-scale fluctuations. In this way, a spontaneous feedback system is established at the plasma edge [15]. This system controls blob/hole formation as well as zonal flow generation.

Experiments were carried out in the boundary plasma of the Joint European Torus (JET) tokamak using a fast reciprocating Langmuir probe array located on the low field side upper part of the device. This probe array allows the simultaneous measurement of the Π_{Re}, density and electric field fluctuations and turbulent particle flux [16]. Measurements were performed in ohmic deuterium plasmas in the limiter configuration, with a magnetic field B~2.4 T at the axis $R_0 = 2.95$m, plasma current I_p~2.2MA, and central-line averaged density $\bar{n} \sim 2\times10^{19}\mathrm{m}^{-3}$. The electron density, temperature and safety factor at the Last Closed Flux Surface (LCFS, $r_{LCFS} = 1.04m$) was $\bar{n} \sim 5\times10^{18}\mathrm{m}^{-3}$, T_e~40eV and q~3.95, respectively. The LCFS was in contact with the high-field-side limiter. The near SOL ($0 < \Delta r \equiv r - r_{LCFS} < 3cm$) has long parallel connection length $\mathrm{L}_{\|} \sim \pi q R_0$ and moderate collisionality $v^*_{ei} \equiv L_{\|}/\lambda_{ei} > 10$, where λ_{ei} is mean free path of electrons. In far SOL ($\Delta r > 3cm$) plasma is in the shadow region of the ICRF-antenna limiter.

2. EDGE-SOL TURBULENCE MEASUREMENTS

The profile of time-averaged ion saturation current $I_s \propto n\sqrt{T_e + T_i}$ is displayed in Fig.1(a). A barrier (steep pressure profile region) can be seen at plasma edge $-2 < \Delta r < -1cm$. At the same location there is a poloidal velocity shear layer, indicated by a steep dropping of floating potential ϕ_f in Fig.1(b). The poloidal phase velocity V_θ of fluctuations is shown in Fig.1(c). Inside the ESL the fluctuations propagate in the electron diamagnetic direction at a speed of ~1 km/s. In the SOL, the poloidal velocity is close to the background **E×B** drift velocity. The central pressures of blobs and holes are also shown in Fig.1(a) as indicated by the peak and valley points of I_s. Projecting the central pressure onto the background profile defines a blob/hole "birth zone" [9]. On each side of the "birth zone" the newly born blobs and holes have the same central pressure. It is consistent with the interchange picture because these blobs and holes could have acquired their pressure only by interchange with the background profile. The "birth zone" coincides with the steep pressure profile region, where the linear growth rate of curvature-driven drift-interchange instability is largest. Therefore the data are consistent with the picture that blobs/holes arise from the nonlinear saturation of linear instabilities at the plasma edge [9].

The radial profiles of skewness and kurtosis of I_s are shown in Fig.1(f) and Fig.1(g). The presence

of negative skewness region coincides with previous observations from DIII-D tokamak [17], where it was reported that this region was near the LCFS. Here we show that the skewness crosses zero exactly at the ESL. Negative skewness implies the accumulation of holes. This region is characterized by a negative tail in the Probability Density Functions (PDF). Outside the ESL the PDF exhibits a positive tail and within the ESL the PDF is near-Gaussian. The parallel dissipation time in the hole-accumulated region is just the conductive time, $\tau_{cond} \approx L_{\|}^2/\chi_{e\|} \sim 20\mu s$, which defines the upper limit of the hole lifetime, where $\chi_{e\|}$ is parallel electron thermal conductivity. If a hole moves radially at a speed 1km/s, it can penetrate 2cm inwards at most. This bounds the region of hole propagation. So the hole-accumulated region can only be a very narrow layer. The skewness will vanish again inside the barrier, as indicated in Fig.1(f).

The perpendicular correlation lengths L_c of turbulence are significantly reduced by the flow shear, as shown in Fig.1(d). The reduction of L_c is mainly caused by the suppression of meso-scale fluctuations at the plasma edge. In the SOL the poloidal correlation length $L_{c\theta}$ is close to the average blob size δ_b, calculated as $\delta_b \approx |V_\theta|\tau_b$ (under the assumption of $|V_\theta| >> |V_r|$, where V_θ and V_r are poloidal and radial velocity of a blob), where f_b is the average duration of pulse events as seen in the I_s signal. In the near SOL $\delta_b \sim L_{c\theta} \sim L_{cr} \sim 2cm$, implying that blobs are elongated in the poloidal direction with an aspect ratio of 2. $L_{c\theta}$ and L_{cr} both decrease towards the wall and in the far SOL they are comparable, $\delta_b \sim L_{c\theta} \sim L_{cr} \sim 0.5cm$, indicating that the blobs tend to be isotropic there, i.e. their aspect ratio approaches unity. The autocorrelation times τ_a are also significantly reduced in the barrier region, see Fig.1(e), as a result of the strong suppression of meso-scale fluctuations.

3. WAVELET ANALYSIS OF THE TURBULENCE DATA

To extract the meso-scale coherent structures wavelet decomposition technique [18, 19] is applied to the probe signals. The meso-scale component contains most information of the blobs and dominates the intermittency, while the small-scale component has a very short autocorrelation time, $\tau_a \sim 3ms$, corresponding to a L_c shorter than the probe separation $5mm$. The degree of coupling to drift waves is reflected in the phase shift between pressure and potential fluctuations, as indicated by the phase shift between I_s and ϕ_f in Fig.2(f). In the interchange limit the phase shift is close to $\pi/2$, as interchange drive is locally balanced by plasma inertia (polarization); in the drift-wave limit the phase shift is nearly zero, as the free streaming of adiabatic electrons causes parallel short circuit. For meso-scale structures observed in the range $-1 < \Delta r < 2cm$, where $L_{\|} \approx \pi q R_0$ is very long, the phase shift is close to $\pi/2$, indicating the coupling to drift wave is weak and the dynamics are close to interchange limit. For the small-scale structures in the same range the two fluctuations are nearly in phase, indicating a strong coupling. This could be a result of the short parallel scale length in a field with magnetic shear $\lambda_{\|} \approx L_s/xk_y$, where $\lambda_{\|}$ is parallel wavelength, k_y is azimuthal wave number, L_s is magnetic shear length and x is the radial space to a mode rational surface. In the limiter shadow the phase shift is significantly modified due to the short-circuit effect of the sheath [1].

The skewness of the meso-scale component is very close to the original skewness, as shown in

Fig.2(g), justifying the argument that intermittency is mainly induced by the meso-scale coherent structures. The skewness profile of the small-scale crosses zero at $\Delta r \approx -1.5cm$. The positive and negative skewness regions of small-scale are produced by positive and negative small wave crests, respectively. On account of their short lifetime, the small structures cannot finger out of the ESL or generate blobs, so that the skewness vanishes in the range $-0.5 < \Delta r < 2cm$. The Root-Mean-Square (rms) fluctuation levels of I_s and ϕ_f are shown in Fig.2(a) and (b). Except in the barrier region the total fluctuations are dominated by the meso-scale. The relative fluctuation level of small-scale turbulence is low, only around 10%. In the barrier region the fluctuation levels of meso-scale are strongly suppressed by the flow shear, however those of small-scale increase. The increase of small-scale fluctuation levels is due to the enhanced instability drive in the steep pressure-profile region and the short lifetime of small-scale turbulent structures. Only those big and stable structures with sufficiently long lifetime $\tau_{life} \geq \tau_{shear}$ [13] are strongly tilted by the flow shear. In this experiment the critical shear decorrelation rate $\omega_{shear} \equiv 2\pi/\tau_{shear}$ in the ESL is ~$200kHz$. This rate defines a boundary between meso-scale and small-scale. In the barrier region fluctuations with frequency below this value are suppressed. The lifetime of small-scale structures is so short that the shear decorrelation is ineffective, and the structures die before they can be significantly tilted. Consequently, the small-scale fluctuations are not suppressed. However, for those meso-scale coherent structures at the plasma edge which are strongly tilted, the associated fluctuations are significantly suppressed, and they therefore make a predominant contribution to the interaction between turbulence and zonal flows.

The rms fluctuation levels of poloidal and radial **E×B** velocities of small-scale drift-wave turbulence and meso-scale coherent structures are shown in Fig.2(c) and (d), respectively. The **E×B** velocity fluctuation levels reflect the internal electric field amplitudes associated with the turbulent structures. For small-scale, in the entire boundary region v_θ and v_r rms-levels are comparable, implying small-scale turbulent eddies are nearly isotropic and seem to be insensitive to the flow shear. For meso-scale, although ϕ_f rms-levels strongly suppressed in the barrier region the **E×B** velocity rms-levels do not vary accordingly. The v_θ rms-level peaks at the position where velocity shear maximizes and in the flow-shear region v_θ rms-level is higher than v_r. This is consistent with structure titling. The tilting of meso-scale coherent structure modifies the internal polarization direction and induces an internal E_r in addition to the azimuthal polarization and E_θ (due to interchange drive). Only in the shadow region v_θ and v_r rms-levels are comparable because of the weak flow shear and short-circuit effect by the sheath.

The radial profiles of Π_{Re} are shown in Fig.2(e). Negative value in the entire boundary region means that the momentum flux is in one direction: outward transport of ion-direction momentum or inward transport of electron-direction momentum. The Π_{Re} is dominated by the meso-scale fluctuations. Only in the barrier region Π_{Re} of small-scale slightly increases and the increase is only due to the enhanced fluctuation levels, see Fig.2(c), not the coherence. The Π_{Re} profile exhibits a "well" structure in the ESL, reaching maximum at the location where turbulent structures are most strongly tilted. The topic of flow driven by turbulent Reynolds stress has been previously investigated

in the JET tokamak [20] and TJ-II stellarator [21]. In this work we mainly concentrate on its relationship to the blob/hole formation.

4. CONDITIONAL AVERAGING OF THE TURBULENCE DATA

To separate these meso-scale coherent objects from other fluctuations, conditional averaging tools [17] are applied. Several thresholds (0.5, 1, 1.5, 2, 2.5 ×rms-level) are used to discriminate the intermittent structures with different amplitude. The existence of an event in the ion saturation current signal is used as the condition to select time slices in the other signals at the same time. By comparing Fig.3(a) and (b), one can see that the initial positive and negative wave crests have a similar size and amplitude. Interchange drive makes the positive and negative wave crests move outwards and inwards, respectively, as shown in Fig.3(c) and (d). As a result of the tilting of the structures in the ESL, the internal polarization direction is modified and an internal E_r is produced, driving the structure to move poloidally, see Fig.3(e) and (f). In the plasma frame of reference positive and negative wave crests move in the ion and electron diamagnetic direction, respectively. Since they move in the opposite direction, they are disconnected and become isolated structures. Finally accumulated regions of blobs and holes are formed on each side of the ESL. When the blobs move into the SOL, where flow shear is not as strong as that in the ESL, the internal polarization is predominantly in the poloidal direction, pushing them to move outwards [4], see Fig.3(i). Besides, a background polarization in the radial direction imposed by the sheath drives a global **E×B** rotation in the ion diamagnetic direction, advecting blobs poloidally. In the near SOL the higher the blob amplitude the faster the radial movement [4], see Fig.3(g) and (i). Fig.3(k) shows the effective radial velocity, defined as $V_r^{eff} \equiv \Gamma/\langle n\rangle$ (proportional to particle flux). Fig.3(m) shows the Π_{Re} (momentum flux). The newly-formed blobs transport momentum as well as particles into the SOL. The higher the blob amplitude the more momentum and particles are carried by the blob. In the hole-accumulated region the relatively high parallel thermal conductivity $\chi_{e\|}$ and the resultant fast parallel extension of the filament structure make the newly born holes much smaller than the newly born blobs, as shown in Fig.3(h). They move inwards but with a much smaller velocity, see Fig.3(j). The associated particle and momentum fluxes are also very small, see Fig.3(l) and (n).

5. MOMENTUM TRANSPORT AND ZONAL FLOW GENERATION

The total momentum flux is composed of Π_{Re}, passive momentum flux carried by the particle transport and high order term, $\langle nv_r v_\theta\rangle = \langle n\rangle\Pi_{\mathrm{Re}} + \langle v_\theta\rangle\Gamma + \langle \tilde{n}\tilde{v}_r\tilde{v}_\theta\rangle$ [9]. The profiles of total momentum flux and passive momentum flux are plotted in Fig.4(a). Compared with the Π_{Re} profile shown in Fig.2(e), the passive momentum flux and the high order term are small in this experiment. The effective momentum diffusivity in the ESL can be calculated as $D \equiv -\langle nv_r v_\theta\rangle/\partial_r \langle nv_\theta\rangle \sim -4\mathrm{m}^2\mathrm{s}^{-1}$, negative means up the gradient. This diffusivity is of the same order of the Bohm diffusivity. The profile of the effective radial velocity is displayed in Fig.4(b), indicating the turbulent particle flux is significantly suppressed in the barrier region and shadow region.

Zonal flows are driven by the divergence of the total momentum flux, $\partial_r \langle n v_r v_\theta \rangle$ [9]. It changes sign at the same position where the poloidal velocity changes direction, as shown in Fig.4(c). Inside this cross-zero point it drives the plasma rotation in the electron direction and outside this point in the ion direction, coinciding with the poloidal velocity profile in the boundary region. In the SOL zonal flows are strongly dissipated by the sheath, because the zonal-flow dynamic time scale is much longer than the sheath dissipation, or convective time scale $\tau_{conv} \equiv L_{\|}/c_s$, where c_s is ion sound speed. This explains why in the SOL the time-averaged floating potential is clamped to zero (plasma potential, $\phi = \phi_s + \phi_f$ where $\phi_s \sim 3T_e$ is the sheath potential), as shown in Fig.1(b). The energy transfer rate between turbulence and zonal flows is formulated as $P \equiv \langle n v_\theta \rangle \, \partial_r \langle n v_r v_\theta \rangle / \langle n \rangle^2$ [10]. In the whole boundary region $P < 0$, as shown in Fig.4(d), negative means energy is transferred from the turbulence to the zonal flows. The zonal-flow energy mainly comes from the meso-scale coherent structures. The skewness and kurtosis of momentum flux is much larger than the particle flux in the vicinity of the ESL, as indicated in Fig.4(e) and (f), suggesting that the momentum transport is more intermittent and more dependent on the meso-scale coherent structures near the "birth zone" of blobs and holes.

CONCLUSIONS

In conclusion, the inherent relationship between blob/hole formation and zonal flow generation is demonstrated. On the one hand, blobs and holes are born in the ESL where zonal flows shear off meso-scale coherent structures, leading to disconnection of positive and negative wave crests, and the blob/hole formation process is spontaneously controlled by the zonal-flow shear. On the other hand, the radial transport of azimuthal momentum and zonal-flow generation is predominantly induced by a tilting of the meso-scale coherent structures, and the newly-formed blobs carry azimuthal momentum up the gradient of the azimuthal flow and drive the zonal-flow shear while moving outwards. In this way, a spontaneous feedback system is established at the plasma edge. This system controls blob/hole formation as well as zonal flow generation. These experimental results present a preliminary answer for: where and how are blobs/holes formed? And what controls the generation rate and initial size of blob? The identification of hole-accumulated region excludes the possibility that the blobs are originated from avalanches developed somewhere deeper in the core region and ultimately coming to the edge [22]. The investigation on the zonal-flow generation casts some new light on the mechanism underlying the spontaneous momentum source at the plasma edge. The concept of the blob/hole formation as a result of turbulence/zonal-flow interaction presents a natural explanation for the universality of the coherent-structure and intermittency phenomena in magnetized plasma turbulence.

ACKNOWLEDGMENTS

This work, supported by the European Communities under the contract of Association between EURATOM/UKAEA, the National Natural Science Foundation of China under Grant No 10605028,

No 10721505 and No 10725523, the KC Wong Foundation of the UK Royal Society, and the President Foundation of CASHIPS, was carried out within the framework of the European Fusion Development Agreement. The views and opinions expressed herein do not necessarily represent those of the European Commission.

REFERENCES

[1]. Krasheninnikov S.I., D'Ippolito D.A. and Myra J.R. 2008 *J. Plasma Phys.* **74** 679

[2]. Pimenta A.A. *et al* 2007 *Geophys. Res. Lett.* **34** L02820

[3]. Fundamenski W. *et al* 2007 *Plasma Phys. Control. Fusion* **49** R43

[4]. Garcia O.E., Bian N.H. and Fundamenski W. 2006 *Phys. Plasmas* **13** 082309; Garcia O.E. *et al* 2005 *Phys. Plasmas* **12** 090701; Garcia O.E. *et al* 2005 *Phys. Plasmas* **12** 062309; Garcia O.E. *et al* 2004 *Phys. Rev. Lett.* **92** 165003

[5]. Garcia O.E. *et al* 2007 *Nucl. Fusion* **47** 667; Garcia O.E. *et al* 2007 *Plasma Phys. Control. Fusion* **49** B47; Garcia O.E. *et al* 2006 *Plasma Phys. Control. Fusion* **48** L1

[6]. Fundamenski W. *et al* 2007 *Nucl. Fusion* **47** 417

[7]. Furno I. *et al* 2008 *Phys. Rev. Lett.* **100** 055004; Diallo A. *et al* 2008 *Phys. Rev. Lett.* **101** 115005; Podestà M. *et al* 2008 *Phys. Rev. Lett.* **101** 045001; Katz N. *et al* 2008 *Phys. Rev. Lett.* **101** 015003

[8]. Krasheninnikov S.I. and Smolyakov A.I. 2008 *Phys. Plasmas* **15** 055909

[9]. Myra J.R. *et al* 2008 *Phys. Plasmas* **15** 032304; Myra J.R. *et al* 2006 *Phys. Plasmas* **13** 092509

[10]. Garcia O.E. *et al* 2006 *Phys. Scr.* **T122** 89; Garcia O.E. *et al* 2006 *Phys. Scr.* **T122** 104

[11]. Bisai N. *et al* 2005 *Phys. Plasmas* **12** 102515

[12]. Diamond P.H. *et al*. 2005 *Plasma Phys. Control. Fusion* **47** R35

[13]. Serianni G. *et al* 2007 *Plasma Phys. Control. Fusion* **49** B267

[14]. Terry P.W. 2000 *Rev. Mod. Phys.* **72** 109

[15]. Naulin V., Juul Rasmussen J. and Nycander J. 2003 *Phys. Plasmas* **10** 1075

[16]. García-Cortés I. *et al* 2000 *Plasma Phys. Control. Fusion* **42** 389; Gonçalves B. *et al* 2005 *J. Nucl. Mater.* **337-339** 376

[17]. Boedo J.A. *et al* 2003 *Phys. Plasmas* **10** 1670

[18]. Farge M., Schneider K. and Devynck P. 2006 *Phys. Plasmas* **13** 042304

[19]. Xu G.S. *et al*. 2006 *Rev. Sci. Instrum.* **77** 063505; Xu G.S. *et al* 2006 *Rev. Sci. Instrum.* **77** 083505

[20]. Hidalgo C. *et al* 2003 *Phys. Rev. Lett.* **91** 065001; Hidalgo C. *et al* 2003 *J. Nucl. Mater.* **313-316** 863; Sánchez E. *et al* 2005 *J. Nucl. Mater.* **337-339** 296

[21]. Gonçalves B. *et al* 2006 *Phys. Rev. Lett.* **96** 145001; Hidalgo C. *et al* 2006 *Plasma Phys. Control. Fusion* **48** S169

[22]. Sarazin Y. and Ghendrih Ph. 1998 *Phys. Plasmas* **5** 4214

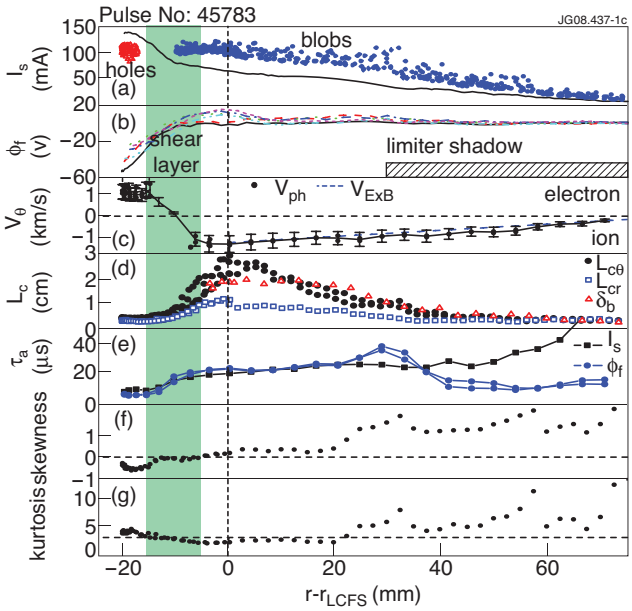

Figure 1: (color online) The radial profiles of (a) ion saturation current I_s, blobs (blue points), holes (red triangles); (b) floating potentials ϕ_f of 6 tips; (c) poloidal phase velocity V_θ of fluctuations and background $\boldsymbol{E}\times\boldsymbol{B}$ drift velocity $V_{E\times B}$; (d) poloidal $L_{c\theta}$ and radial L_{cr} correlation length and average blob size ∂_b; (e) autocorrelation times of I_s and ϕ_f; (f) skewness and (g) kurtosis of I_s.

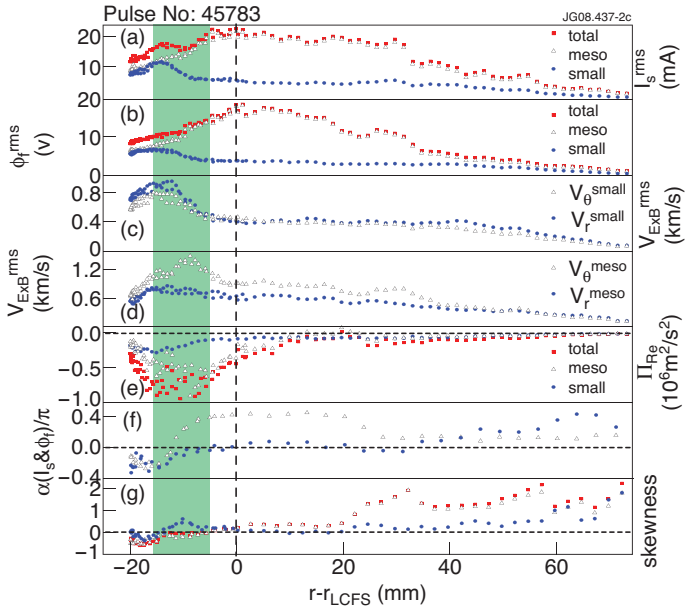

Figure 2: (color online) The radial profiles of (a) rms-levels of I_s fluctuation; (b) rms-levels of ϕ_f fluctuation; (c) rms-levels of small-scale v_θ and v_r fluctuations; (d) rms-levels of meso-scale v_θ and v_r fluctuations; (e) Reynolds stress; (f) phase shift between I_s and ϕ_f; (g) skewness of I_s. Total fluctuation (red squares), meso-scale (black triangles), small-scale (blue points).

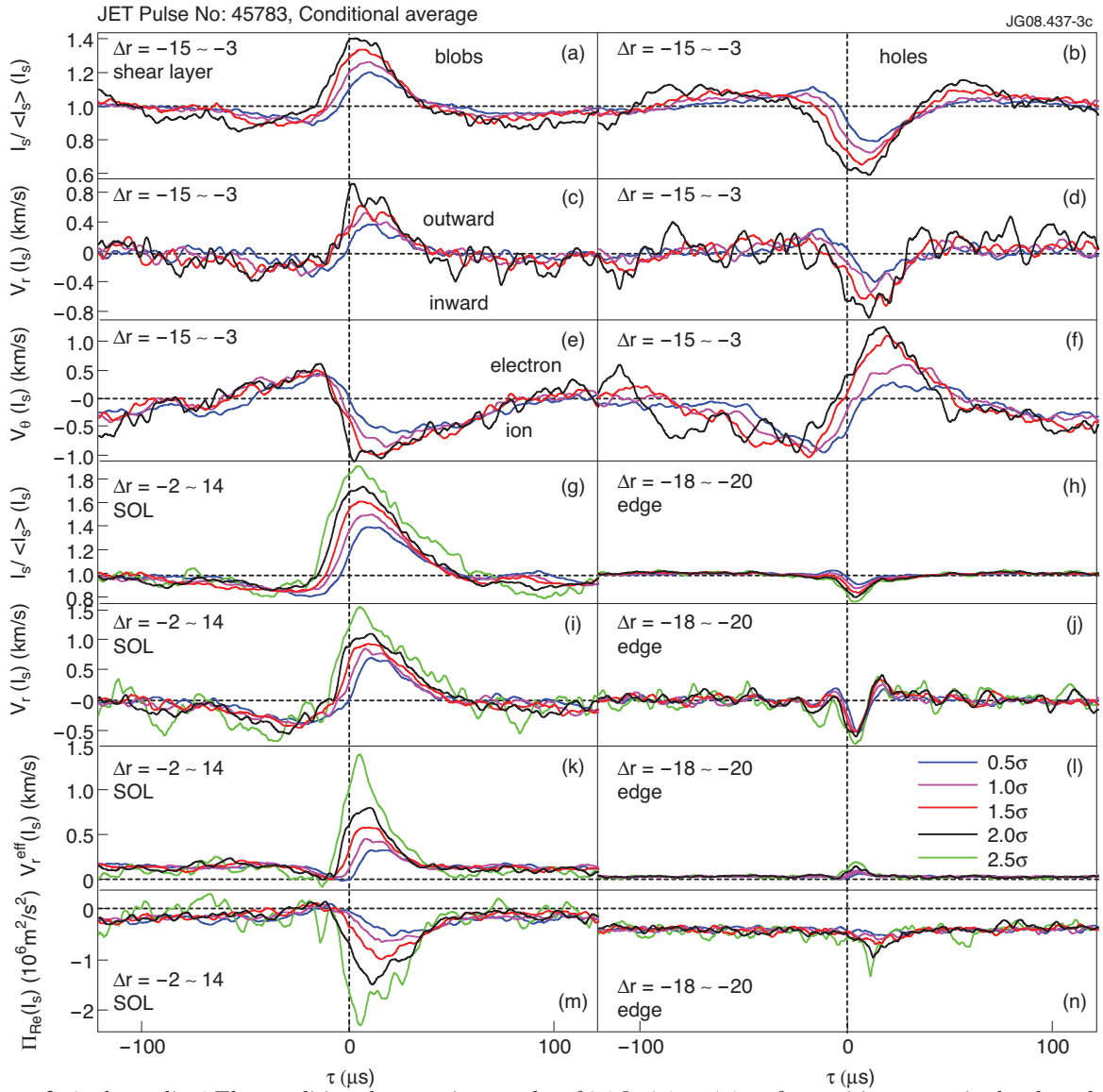

Figure 3: (color online) The conditional averaging results of (a) I_s, (c) v_r, (e) v_θ for positive events in the shear layer; (b) I_s, (d) v_r, (f) v_θ for negative events in the shear layer; (g) I_s, (i) v_r, (k) V_r^{eff}, (m) Π_{Re} for positive events in the near SOL; (h) I_s, (j) v_r, (l) V_r^{eff}, (n) Π_{Re}e for negative events inside the shear layer. 0.5, 1, 1.5, 2, 2.5 ×rms-level thresholds were applied to the I_s to select the events. The systematic shift of peaks is an artificial result of the conditional

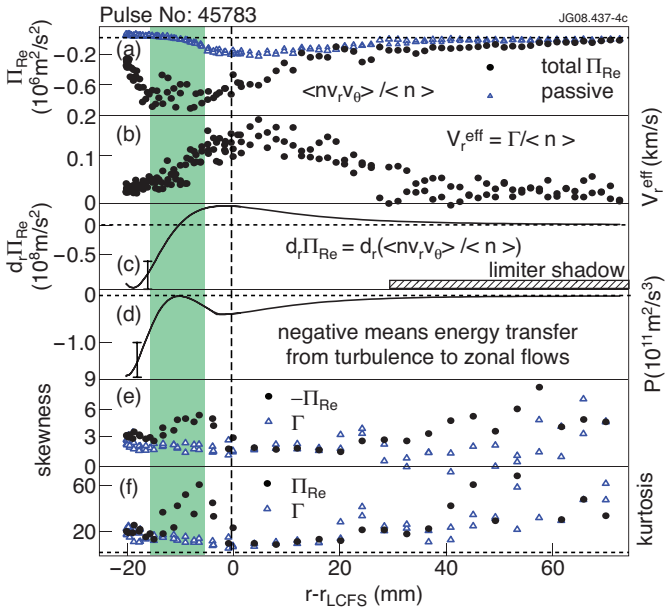

Figure 4: (color online) The radial profiles of (a) total and passive momentum fluxes; (b) effective radial velocity; (c) radial gradient of momentum flux; (d) energy transfer rate between turbulence and zonal flows; (e) skewness and (f) kurtosis of Reynolds stress and particle flux.